International Journal of Automotive Technology, Vol. 20, No. 6, pp. 1103–1112 (2019)
DOI 10.1007/s12239–019–0103–y

pISSN 1229–9138/ eISSN 1976–3832

DISTRIBUTED FORMATION CONTROL OF HOMOGENEOUS VEHICLE PLATOON CONSIDERING VEHICLE DYNAMICS

Liwei Xu, Weichao Zhuang, Guodong Yin* and Chentong Bian

School of Mechanical Engineering, Vehicle Engineering, Southeast University, Nanjing 211189, China

(Received 14 May 2018; Revised 21 February 2019; Accepted 26 March 2019)

ABSTRACT–Vehicle dynamics plays a significant role on the formation of a vehicle platoon, especially at high speed condition. This paper proposes a distributed platoon formation framework for homogeneous autonomous vehicles which takes the vehicle dynamics into consideration. The boundaries of vehicle stability are firstly calculated by considering both lateral dynamics and actuator saturation. By combining the stability boundaries with multi-objective flocking (MOF) algorithm, a distributed formation controller is designed, which can form the vehicle platoon with high cruising speed steadily and rapidly. In addition, a low-level tracking controller is proposed to constitute a hierarchical control architecture which can achieve stable and accurate formation of platoon. Simulation results show the proposed platoon formation controller achieves safe, stable and rapid platoon formation than the traditional MOF-based formation controller which does not consider the vehicle dynamics.

KEY WORDS : Platoon formation control, Homogeneous system, Vehicular dynamic constraints, Autonomous vehicle

1. INTRODUCTION

Traffic safety issue has attracted many attentions since nearly 1.25 million people die each year as a result of roadway crashes (World Health Organization, 2015). Many technologies have been developed to improve vehicle safety, such as electronic stability control system, autonomous vehicle, vehicle platooning and so on. Among them, vehicle platoon, referring to a group of vehicles driving at a harmonized speed with small pre-defined inter-vehicle spacing, could increase traffic capacity, enhance highway safety, and reduce fuel consumption and has been investigated widely (Zhang *et al*., 2011).

Many studies have been conducted to achieve stable and efficient vehicle platoon control, such as spacing policy (Swaroop *et al*., 1994; Zhou and Peng, 2005), optimization of communication topology (Fax and Murray, 2004; Zheng *et al*., 2016), interference rejection (Xu *et al*., 2018) and the affection of communication delay (Ploeg *et al*., 2014; Al-Jhayyish and Schmidt, 2018; Xu *et al*., 2019). Among some kinds of literature above, some researchers investigate the string stability of vehicle platoon, which referred to whether the disturbance will be amplified when propagated downstream along the platoon. Some other pieces of literature use a variety of control methods to achieve string-stable platoon control. Naus *et al*. (2010) and Wang and Nijmeijer (2015) used the PD-controller, while Gao *et al*. (2017) and Ploeg *et al*. (2014) adopted robust control. Also, model predictive control of platoon is proposed by Kamal *et al*. (2014) to achieve better platoon control performance.

In addition to the platooning control, the platoon formation is also crucial, which refers to vehicles moving from different lanes to form the platoon. In the last decade, numerous control strategies were developed to achieve the formation control of the robot and the unmanned aerial vehicle, and some had been applied in vehicle platoon formation control problem. Yang *et al*. (2017) and Peng *et al*. (2016) adopted a consensus-based cooperative control method to achieve the formation of vehicle platoon. Yu and Liu (2016) combined the cascaded system theory and directed graph method to resolve the leader-follower formation problem while considering velocity constraints. Zhang *et al*. (2013) present an integrated controller using the global virtual structure and unity path-tracking controller to address the formation problem of networked nonholonomic mobile vehicles. Another study presented by Desai *et al*. (2001) used the graph theory to develop a modeling framework of the platoon formation. In Antonelli and Chiaverini (2006), the proper task functions in the framework of singularity-robust task-priority inverse kinematics are used to achieve the formation of the vehicle platoon. Another study presented by Bishop (2003) solved the platoon of cooperating vehicles by employing the redundant manipulator technique. Iftekhar (2012) and Liu and Xu (2015) both proposed the distributed vehicle platoon formation protocols based on multi-objective flocking (MOF), which could plan the trajectories of all

**Corresponding author*. e-mail: ygd@seu.edu.cn

vehicles without the crash. Besides, the flocking approach can achieve stable and flexible platoon formation compared to other formation methods (Iftekhar, 2012).

Most researches mentioned above only adopted the vehicle kinematic model or modeled the vehicle as a point-mass system. However, vehicle dynamics cannot be ignored because of the nonlinearity of the vehicle. To the best of our knowledge, few works of literature are focusing on vehicle platoon formation with high cruising speed, from the perspectives of ensuring vehicle stability and improving formation safety and efficiency. This paper focuses on studying the formation control of the homogeneous autonomous vehicles (HAV) with high cruising speed. The contribution of this paper is twofold. First, the vehicle lateral dynamics and actuators saturation are considered in the vehicle platoon formation control problem. Based on the derived stability boundaries, a stable and efficient distributed platoon formation controller (DPFC) is designed by combining the stability boundaries and MOF algorithm. Second, a distributed path-tracking controller is proposed to form a hierarchical control architecture which can achieve stable planning and tracking of platoon formation.

The remainder of this paper is organized as follows: The introduction of MOF is presented in Section 2. Kinematic and dynamic vehicle models are introduced in Section 3. In Section 4, The framework of the hierarchical controller, including planning-level and tracking-level, is designed. Simulation is conducted in Section 5. Finally, Section 6 concludes.

2. FLOCKING CONTROL METHOD

Considering a group of agents

$$\begin{cases} \dot{q}_i = p_i \\ \dot{p}_i = u_i \end{cases} \quad i = 1, 2, ..., n \tag{1}$$

with the neighboring set

$$N_i^t = \{j: \|q_i - q_j\|_\sigma < \mathcal{R}_\sigma, j \neq i\} \tag{2}$$

where q_i, $p_i \in \mathbb{R}^m$ are the position and velocity vectors of agent i, $u_i \in \mathbb{R}^n$ is the control input of agent i, $\mathcal{R}_\sigma$ is the distances that agent i can perceive and communicate with other agents, and $\|\cdot\|_\sigma$ is the vector norm.

According to Olfati-Saber (2006), the input of agent i in the Flocking algorithm can be described as follows:

$$u_i = f_i^\alpha + f_i^r \tag{3}$$

where f_i^α which is denoted by Equation (4) is to regulate the position between agent i and its neighbors such that the collision with each other can be avoided and the cohesion is maintained in a group.

$$f_i^\alpha = \sum_{j \in N_i^t} \phi_\alpha \left(\|q_j - q_i\|_\sigma \right) n_{ij} + \sum_{j \in N_i^t} a_{ij}(p_j - p_i) \tag{4}$$

In Equation (3), f_i^r is responsible for navigational feedback to the uniform virtual leader agent r, which is given by

$$f_i^r \triangleq f_i^r(q_i, p_i, q_r, p_r) \tag{5}$$

Here, n_{ij} is a direction vector from agent i to agent j; $\phi_\alpha(\cdot)$ is the dual power that is derived from the interaction of molecules; $a_{ij}(\cdot)$ is the elements of the adjacency matrix of agent group, and the (q_r, p_r) is the state of a navigational agent. Given the limited space available, the full expressions about $\|\cdot\|_\sigma$, n_{ij}, $\phi_\alpha(\cdot)$, and $a_{ij}(\cdot)$, which can be found in Olfati-Saber (2006), are omitted in this paper.

Furthermore, to generate the vehicle string, Iftekhar (2012) introduced a new navigational control protocol. Different from the agents in Olfati-Saber (2006), each vehicle in the new protocol has its target with the position $\hat{q}_i$ and velocity $\hat{p}_i$. The navigational control protocol for vehicle i is described as

$$f_i^r = -c_1^r(q_i - \hat{q}_i) - c_2^r(p_i - \hat{p}_i) \tag{6}$$

where c_1^r and c_2^r are positive constants. The first component of the above equation is mainly used to follow the middle position (i.e., $\hat{q}_i$), and the second component is used to reach the desired velocity (i.e., $\hat{p}_i$).

3. VEHICLE MODELING

In this paper, two vehicle models, the 2DOF kinematic model, and the 3DOF dynamic model are adopted to construct the planning level and the tracking level, respectively. Since the vehicle platoon system is homogeneous, we use the standard vehicle model to represent each single vehicle model.

3.1. Partially-Linear Kinematic Model

As shown in Figure 1, suppose vehicle is the front wheel steering structure and the sideslip angle β is small, then the kinematic model of the ith vehicle can be expressed as:

$$\begin{cases} \dot{X} = v\cos\theta \\ \dot{Y} = v\sin\theta \\ \dot{\theta} = \omega \end{cases} \tag{7}$$

where (X, Y) are the global coordinates of the mass center; v is the velocity; θ is the heading angle, and ω is the yaw rate.

To use the flocking algorithm, Equation (7) need to be transformed into a point mass model. Denote by ζ_1 and ζ_2 the longitudinal acceleration and yaw acceleration, then Equation (7) is rewritten as

$$\begin{cases} \dot{\mathcal{X}} = (Re_1)v \\ \dot{R} = R\hat{\omega} \\ \dot{v} = \zeta_1 \\ \dot{\omega} = \zeta_2 \end{cases} \tag{8}$$

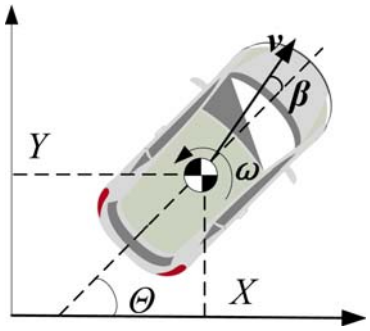

Figure 1. Schematic diagram of vehicle kinematic model.

where $\mathcal{X}=[X,Y]^{\mathrm{T}}$, $R=\begin{bmatrix}\cos\theta & -\sin\theta\\ \sin\theta & \cos\theta\end{bmatrix}$, $e_1=[1,0]^{\mathrm{T}}$.

According to near-identity diffeomorphism (Olfati-Saber, 2002), by using the transformation

$$\mathcal{S}=\mathcal{X}+\lambda(Re_1) \tag{9}$$

Equation (8) can be expressed as:

$$\begin{cases}\dot{\mathcal{S}}=W\\ \dot{W}=\eta\\ \dot{R}=R\hat{\omega}\\ \dot{\omega}=e_2^{\mathrm{T}}\zeta=e_2^{\mathrm{T}}R_{\lambda,}^{-1}\eta-\dfrac{v\omega}{\lambda}\end{cases} \tag{10}$$

where $\zeta=[\zeta_1,\ \zeta_2]^{\mathrm{T}}$; $\lambda=\{\lambda|\lambda\in\mathbb{R},\ 0<\lambda<1\}$; $\mathcal{S}$ and W are the terms of position and velocity of the system (8) in the new coordinate, corresponding to the $\mathcal{X}$ and $[v,\ \omega]^{\mathrm{T}}$; η is the input of a new system; e_2 = $[0,\ 1]^{\mathrm{T}}$; $R_\lambda=\begin{bmatrix}\cos\theta & -\lambda\sin\theta\\ \sin\theta & \lambda\cos\theta\end{bmatrix}$ and $\hat{\omega}=\begin{bmatrix}0 & -\omega\\ \omega & 0\end{bmatrix}$. Further, ζ can be expressed as

$$\begin{aligned}\zeta&=R_\lambda^{-1}\eta-R_\lambda^{-1}R[\lambda\omega^2,\ v\omega]^{\mathrm{T}}\\ &=R_\lambda^{-1}\eta+\begin{bmatrix}\lambda\omega^2\\ -\dfrac{v\omega}{\lambda}\end{bmatrix}\end{aligned} \tag{11}$$

Denoting $\zeta=\tilde{f}(\theta,\ v,\ \omega,\ \eta,\ \lambda)$ and $\xi=[v,\ \omega]^{\mathrm{T}}$. By using the Euler numerical method, if T is the interval, then the yaw rate and longitudinal velocity at time $k+1$ can be expressed as

$$\begin{aligned}\xi(k+1)&=\xi(k)+T\tilde{f}\left(\theta(k),v(k),\omega(k),\eta(k),\lambda(k)\right)\\ &=\begin{bmatrix}v(k)\\ \omega(k)\end{bmatrix}+T\begin{bmatrix}\zeta_1(k)\\ \zeta_2(k)\end{bmatrix}\end{aligned} \tag{12}$$

The first two items of Equation (10), i.e., $(\mathcal{S},W)$ forms the linear subsystem. By applying the MOF algorithm to this linear system, the longitudinal and yaw accelerations can be got by calculating Equation (11). Then, by computing Equation (12), the longitudinal speed and yaw rate of the vehicle at the next time can be gained.

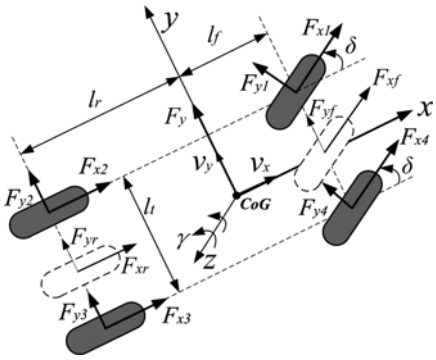

Figure 2. Schematic diagram of vehicle dynamic model.

Remark 1: There are nonlinear relationships between η and ζ. For the convenience of calculation, we apply the Equations (11) and (12) to obtain the relationship between the η and ξ. Then by setting up the tracking controller to track ξ, the real input of a single vehicle that can satisfy the dynamic requests and realize the platoon formation simultaneously can be obtained.

3.2. Vehicle Dynamics

As shown in Figure 2, the traditional 3DOF vehicle model which focus on the plane dynamics that consists of the longitudinal and lateral translations and the rotation around the vertical axis is employed and can be written as follows:

$$\begin{cases}\dot{v}_{\mathrm{x}}=\gamma v_{\mathrm{y}}+\dfrac{1}{M}(F_{\mathrm{X}}-F_{\mathrm{R}})\\ \dot{v}_{\mathrm{y}}=-\gamma v_{\mathrm{x}}+\dfrac{1}{M}F_{\mathrm{Y}}\\ \dot{\gamma}=\dfrac{1}{I_{\mathrm{z}}}[l_{\mathrm{f}}F_{\mathrm{yf}}-l_{\mathrm{r}}F_{\mathrm{yr}}+\dfrac{l_{\mathrm{t}}}{2}(F_{\mathrm{xr}}-F_{\mathrm{xf}})]\end{cases} \tag{13}$$

with

$$\begin{aligned}F_{\mathrm{yf}}&=(F_{\mathrm{x1}}+F_{\mathrm{x4}})\sin\delta+(F_{\mathrm{y1}}+F_{\mathrm{y4}})\cos\delta\\ F_{\mathrm{yr}}&=F_{\mathrm{y2}}+F_{\mathrm{y3}}\\ F_{\mathrm{xf}}&=F_{\mathrm{x1}}\cos\delta-F_{\mathrm{y1}}\sin\delta+F_{\mathrm{x2}}\\ F_{\mathrm{xr}}&=F_{\mathrm{x4}}\cos\delta-F_{\mathrm{y4}}\sin\delta+F_{\mathrm{x3}}\\ F_{\mathrm{X}}&=(F_{\mathrm{x1}}+F_{\mathrm{x4}})\cos\delta-(F_{\mathrm{y1}}+F_{\mathrm{y4}})\sin\delta+F_{\mathrm{x3}}+F_{\mathrm{x2}}\\ F_{\mathrm{Y}}&=(F_{\mathrm{x1}}+F_{\mathrm{x4}})\sin\delta+(F_{\mathrm{y1}}+F_{\mathrm{y4}})\cos\delta+F_{\mathrm{y3}}+F_{\mathrm{y2}}\\ F_{\mathrm{R}}&=Mgk_{\mathrm{r}}+\frac{1}{2}k_{\mathrm{d}}S_{\mathrm{d}}\rho v_{\mathrm{x}}^2\end{aligned}$$

where v_{x} and v_{y} are the longitudinal and lateral velocities. l_{t} is the wheel tread. F_{xi} and F_{yi} are the longitudinal and lateral tire forces, where i = 1, 2, 3, 4 are left-front, left-rear, right-rear, and right-front wheels. M and I_{z} are the vehicle mass and the moment of inertia. l_{f} and l_{r} are the front and

rear center of gravity (CoG) distances. δ is front steering angle. γ is the yaw rate. F_X and F_Y are the longitudinal and lateral resultant forces at the CoG. g is the acceleration of gravity. k_r and k_d are the rolling resistance coefficient and the air resistance coefficient. ρ is the air density and S_d is the windward area.

Remark 2: It should be noticed that the longitudinal tire force F_{xi} in vehicle dynamic model is the longitudinal tire resultant force, and its generation is different for four-wheel independent drive electric vehicles (4WID-EV) and other types of vehicles. For the 4WID-EV, F_{xi} can be realized by directly controlling the torque of the motors. However, for other types of automobiles, such as the internal combustion engine vehicles and centralized drive electric vehicles, it is difficult to obtain F_{xi} by using mechanical connection due to the mechanical transmissions complexity. A straightforward way is by the vehicle stability control system, that is, to add a different braking moment to different wheels.

Let C_f and C_r denote the front and rear tire cornering stiffness. If the tire sideslip angles are small, the lateral tire forces can be approximated as

$$\begin{cases} F_{y,m} = C_f\left(\delta - \dfrac{1}{v_x}(\gamma l_f + v_y)\right), & m = 1, 4 \\ F_{y,n} = \dfrac{C_r}{v_x}(v_y - \gamma l_r), & n = 2, 3 \end{cases} \tag{14}$$

Denote by $\varsigma = [v_x, v_y, \gamma]^T$ the state of vehicle dynamic system and $u = [F_{x1}, F_{x2}, F_{x3}, F_{x4}, \delta]^T$ the control input. The vehicle dynamic model in the form of discrete time can be written as

$$\varsigma(k+1) = \bar{f}(T, \varsigma(k), u(k)) \tag{15}$$

where T is the discrete time step and

$$\bar{f} = \begin{bmatrix} v_x(k) + T\left(\gamma(k)v_y(k) + \dfrac{1}{M}(F_X(k) - F_R(k))\right) \\ v_y(k) + T\left(-\gamma(k)v_x(k) + \dfrac{1}{M}F_Y(k)\right) \\ \gamma(k) + \dfrac{T}{I_z}[l_f F_{yf}(k) - l_r F_{yr}(k) + \dfrac{l_t}{2}(F_{xr}(k) - F_{xf}(k))] \end{bmatrix}$$

Let $\bar{\varsigma}_{k+1}$ be the state trajectory obtained by applying the input $\bar{u}_k = u(k-1)$ to the system (15) at the time k with $\bar{\varsigma}_k = \varsigma(k)$. Then, it can be expressed as

$$\bar{\varsigma}_{k+1} = \bar{f}(T, \bar{\varsigma}_k, \bar{u}_k) \tag{16}$$

Note that, the reference state $\bar{\varsigma}_k$ obtained by Equation (16) and input $\bar{u}_k$ are the stable points of the nonlinear vehicle dynamic system. In the light of Equation (16), the continuous nonlinear system (15) can be transformed into a linear time-varying (LTV) system by linearized at each time step k around the point $(\bar{\varsigma}_k, \bar{u}_k)$ as follows:

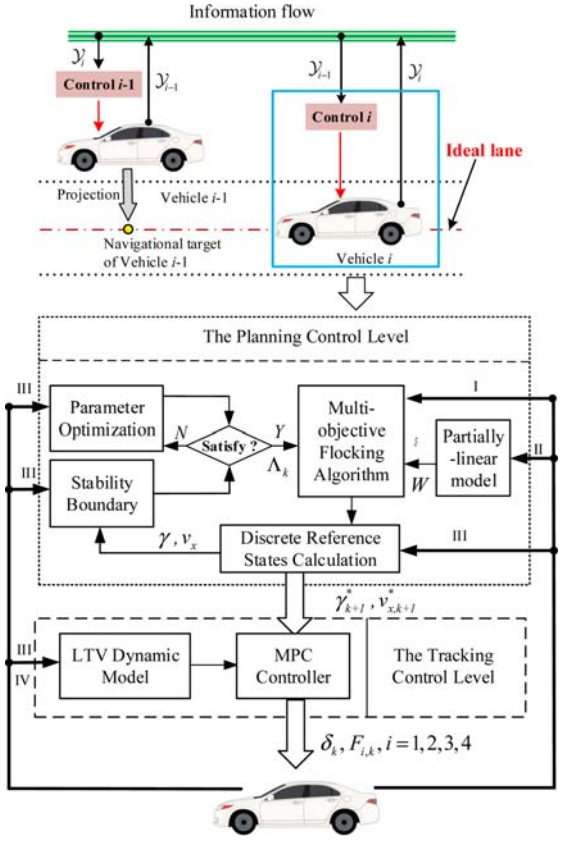

Figure 3. Distributed control framework of the platoon formation control system. I indicates the information of navigational target and neighborhood vehicles; II represents X, Y and θ; III means γ and v_x; IV is δ and F_{xi}; $\mathcal{Y}_i$ and $\mathcal{Y}_{i-1}$ mean the information of vehicles i and $i-1$ that needs to be transmitted through the communications (i.e., the position, speed and heading angle of the vehicle).

$$\varsigma(k+1) = A_k\varsigma(k) + B_k u(k) + d_k \tag{17}$$

with

$$d_k = \bar{\varsigma}_{k+1} - A_k\bar{\varsigma}_k - B_k\bar{u}_k$$

$$A_k = \frac{\partial \bar{f}}{\partial \varsigma}\Big|_{\bar{\varsigma}_k, \bar{u}_k} = \begin{bmatrix} \dfrac{a_1}{M} & \gamma + a_2 & v_y + a_3 \\ -\gamma - \dfrac{a_4}{M} & \dfrac{a_5}{M} & -v_x - \dfrac{a_6}{M} \\ \dfrac{a_7}{I_z} & -\dfrac{a_8}{I_z} & \dfrac{a_9}{I_z} \end{bmatrix}_{\bar{\varsigma}_k, \bar{u}_k}$$

$$B_k = \frac{\partial \bar{f}}{\partial u}\Big|_{\bar{\varsigma}_k, \bar{u}_k} = \begin{bmatrix} \dfrac{\cos\delta}{M} & \dfrac{1}{M} & \dfrac{1}{M} & \dfrac{\cos\delta}{M} & \dfrac{-b_1}{M} \\ \dfrac{\sin\delta}{M} & 0 & 0 & \dfrac{\sin\delta}{M} & \dfrac{b_2}{M} \\ \dfrac{b_3}{I_z} & -\dfrac{l_t}{2I_z} & \dfrac{l_t}{2I_z} & \dfrac{b_4}{I_z} & \dfrac{b_5}{I_z} \end{bmatrix}_{\bar{\varsigma}_k, \bar{u}_k}$$

where $a_1 = \frac{2C_f(v_y+\gamma l_f)\sin\delta}{v_x^2} + S_d k_d \rho v_x$, $a_2 = \frac{2C_f \sin\delta}{Mv_x}$, $a_3 = \frac{2C_f l_f \sin\delta}{Mv_x}$, $a_4 = \frac{2C_r(v_y-\gamma l_r)}{v_x^2} - \frac{2C_f(v_y+\gamma l_f)\cos\delta}{v_x^2}$, $a_5 = \frac{2C_r - 2C_f\cos\delta}{v_x}$, $a_6 = \frac{2C_r l_r}{v_x} + \frac{2C_f\cos\delta}{v_x}$, $a_8 = \frac{2C_r l_r}{v_x} + \frac{2C_f l_f\cos\delta}{v_x}$, $a_9 = \frac{2C_r l_r^2}{v_x} - \frac{2C_f l_f^2\cos\delta}{v_x}$, $a_7 = \frac{2C_f l_f(v_y+\gamma l_f)\cos\delta}{v_x^2} + \frac{2C_r l_r(v_y-\gamma l_r)}{v_x^2}$, $b_1 = (F_{x1}+F_{x4}-2C_f)\sin\delta + \frac{2C_f(v_x\delta - v_y + \gamma l_f)}{v_x}\cos\delta$, $b_3 = \frac{1}{2}l_t\cos\delta - l_f\sin\delta$, $b_2 = (F_{x1}+F_{x4}+2C_f)\cos\delta - \frac{2C_f(v_x\delta - v_y+\gamma l_f)}{v_x}\sin\delta$, $b_4 = \frac{1}{2}l_t\cos\delta + l_f\sin\delta$, $b_5 = \frac{l_t}{2}(F_{x1}+F_{x4})\sin\delta + l_f[(F_{x1}+F_{x4})\cos\delta + 2C_f(\cos\delta - (\delta - \frac{v_y+\gamma l_f}{v_x})\sin\delta]$

4. DISTRIBUTED PLATOON FORMATION CONTROLLER DESIGN

In this section, based on the MOF algorithms, a hierarchical DPFC for the autonomous vehicles is established. The whole controller is divided into two control levels: planning control level and tracking control level. The architecture of the whole control system is shown in Figure 3.

In planning control level, the reference states that satisfy the vehicle lateral stability constraints is generated, and the MOF method is used to derive the reference trajectory for each vehicle. In the lower level, the distributed model predictive controller is designed to track the reference states and ensure each vehicle's stability.

4.1. Plan-level Controller Design

To introduce the vehicle dynamics, the vehicle stability boundaries about the yaw rate and longitudinal velocity are established firstly.

4.1.1. Stability boundaries

Vehicle lateral acceleration in Equation (13) can be rewritten as

$$a_y = \gamma v_x + \dot{v}_y \tag{18}$$

Due to $v_y = v_x\tan\beta$, the above equation can be re-expressed as:

$$a_y = \gamma v_x + \dot{v}_x\tan\beta + \frac{v_x\dot{\beta}}{\sqrt{1+\tan^2\beta}} \tag{19}$$

Assuming both of β and $\dot{\beta}$ are small, the maximal value of yaw rate which is given by Rajamani (2011) can be described as

$$\gamma_{max} = 0.85\frac{\mu_g g}{v_x} \tag{20}$$

where μ_g is the tire-road adhesion and is presumed invariable. In this paper, as the linear tire model is employed, the maximum of lateral acceleration should not be surpassed 0.4 g. Therefore, the maximal value of the yaw rate is rewritten as

$$\gamma_{max} = 0.85\frac{0.4g}{v_x} = \frac{0.34g}{v_x} \tag{21}$$

As a consequence, the constraint conditions about yaw rate can be signified as

$$-\gamma_{max} \le \gamma \le \gamma_{max} \tag{22}$$

Furthermore, according to Jia (2000), the longitudinal acceleration a_x can guarantee that the vehicle wheels are not lifting from the ground, and should satisfy the following condition:

$$-\frac{gl_f}{h_g} \le a_x \le \frac{gl_r}{h_g} \tag{23}$$

where h_g is the height of CoG.

In reality, to prevent the phenomena of sideslip and track slip arising, the longitudinal force F_X and lateral force F_Y should not exceed maximum frictional force that the ground can afford, i.e., as shown in Figure 4, the longitudinal and lateral forces should abide by the following inequality constraint:

$$F_X^2 + F_Y^2 \le (\mu_g Mg)^2 \tag{24}$$

Combining Equations (23) and (24), the range of longitudinal acceleration can be represented as:

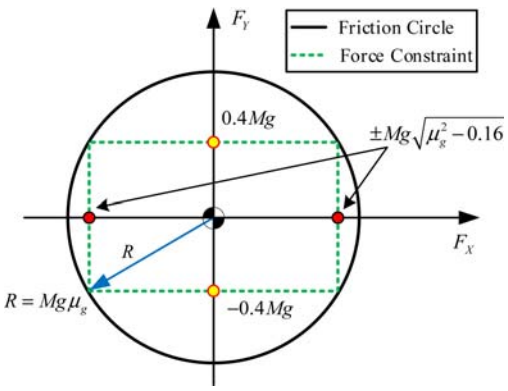

Figure 4. Tire force constraint.

$$a_{\mathrm{x,min}} \le a_{\mathrm{x}} \le a_{\mathrm{x,max}} \tag{25}$$

where $a_{\mathrm{x,min}} = \max\left(-g\sqrt{\mu_{\mathrm{g}} - 0.16},\ -\frac{gl_{\mathrm{f}}}{h_{\mathrm{g}}}\right)$ and $a_{\mathrm{x,max}} = \min\left(g\sqrt{\mu_{\mathrm{g}} - 0.16},\ \frac{gl_{\mathrm{f}}}{h_{\mathrm{g}}}\right)$. Then, the range of longitudinal velocity is obtained

$$\tilde{v}(k) - Ta_{\mathrm{x,min}} \le v_{\mathrm{x}} \le \tilde{v}(k) + Ta_{\mathrm{x,max}} \tag{26}$$

where $\tilde{v}(k)$ is the longitudinal velocity at the moment k.

Algorithm 1: The Optimization Flow

1 **if** $t = 0$ **then**
  Random generated $\tilde{\Lambda}_0$ in the allowable ranges;
  else
  $\tilde{\Lambda}_{\mathrm{t}} = \Lambda_{\mathrm{t-1}}$;
  end if

2 Calculate the yaw rate γ and longitudinal velocity v_{x} based on Equations (3-6) and Equation (10-12) and Optimized variables $\Lambda_0/\tilde{\Lambda}_{\mathrm{t}}$

3 **if** γ and v_{x} satisfy Equations (22) and (26) **then**
  Optimized variables are the parameters of Flocking algorithm at this time, i.e., $\Lambda_0 = \tilde{\Lambda}_0$ and $\Lambda_{\mathrm{t}} = \tilde{\Lambda}_{\mathrm{l}}$, and go to **5**;
  else
  Go to **4**;
  end if

4 Regenerate the new optimized variables $\tilde{\Lambda}_0/\tilde{\Lambda}_{\mathrm{t}}$ by solving the optimization problem (30) and go to **2**;

5 γ and v_{x} are the reference states, i.e, $\gamma^*_{\mathrm{k+1}} = \gamma$, $v^*_{\mathrm{x,k+1}} = v_{\mathrm{x}}$, output the $\gamma^*_{\mathrm{k+1}}$ and $v^*_{\mathrm{x,k+1}}$

4.1.2. Multi-objective Flocking Optimization

After obtaining the stability boundaries, the next work is to restrict the output of the planning controller not out of the ranges.

Based on the proposed MOF in Section 2, there are four parameters, named as $\mathcal{G}_{\mathrm{a}}$, $\mathcal{G}_{\mathrm{b}}$, c_1^r and c_2^r, can affect the values of the output of the planning controller. $\mathcal{G}_{\mathrm{a}}$ and $\mathcal{G}_{\mathrm{b}}$ are related with ϕ_α and may affect the acting forces between agents, and the parameters c_1^r and c_2^r connect with the navigational force.

Moreover, for the multi-vehicle system, the terms $q_{\mathrm{i}} - \hat{q}_{\mathrm{i}}$ and $p_{\mathrm{i}} - \hat{p}_{\mathrm{i}}$ in Equation (6) directly relate to the position, yaw rate and longitudinal velocity of the vehicle, hence it is inappropriate to apply two constants to restrain $q_{\mathrm{i}} - \hat{q}_{\mathrm{i}}$ and $p_{\mathrm{i}} - \hat{p}_{\mathrm{i}}$. Accordingly, in this paper, two parametric diagonal matrices are used, and the Equation (6) is rewritten as

$$f_i^r = -\mathcal{P}_1^r(q_i - \hat{q}_i) - \mathcal{P}_2^r(p_i - \hat{p}_i) \tag{27}$$

where $\mathcal{P}_1^{\mathrm{r}} = \begin{bmatrix} p_{11} & 0 \\ 0 & p_{12} \end{bmatrix}$ and $\mathcal{P}_2^{\mathrm{r}} = \begin{bmatrix} p_{21} & 0 \\ 0 & p_{22} \end{bmatrix}$ are the parametric diagonal matrices, in which p_{11}, p_{12}, p_{21}, p_{22} are positive constants. Let $\Lambda = [\mathcal{G}_{\mathrm{a}}, \mathcal{G}_{\mathrm{b}}, p_{11}, p_{12}, p_{21}, p_{22}]^{\mathrm{T}}$, then Λ is the optimal variable matrix.

Since the purpose of optimization about Flocking algorithm is to limit the output of the planning controller, i.e., the values of longitudinal velocity and yaw rate, the objective of optimization is written as

$$J_1 : \sum_{\mathrm{k=1}}^{\mathrm{N_t}} \left(P_1 \left\| v_{\mathrm{x,k}} - V_{\mathrm{k}} \right\|_2^2 + Q_1 \left\| \gamma_{\mathrm{k}} - \gamma_{\mathrm{max,k}} \right\|_2^2 \right) \tag{28}$$

where P_1 and Q_1 are weight coefficients; N_{t} is a constant, and V_{k} is the maximum of velocity that can be represented by the following equation:

$$V_{\mathrm{k}} = \begin{cases} v(k) + Ta_{\mathrm{x,max}},\ a_{\mathrm{x}} > 0 \\ v(k) - Ta_{\mathrm{x,min}},\ a_{\mathrm{x}} \le 0 \end{cases} \tag{29}$$

Remark 3: For the cost function J_1, it is evident that the time of realizing the formation would take longer when the outputs of planning-controller approach the origin strictly. In order to generate a balance between the control performance and efficiency, the maximum longitudinal speed and yaw rate are adopted to construct the J_1. Combining with the dynamic constraints (22) and (26), the function of J_1 is to propel the v_{x} and γ_{max} to approach the maximums but not exceeding stability boundary.

When the stability boundaries and cost function have been confirmed, the following optimization problem is solved:

$$\min_{\Lambda} J_1 \tag{30}$$

$$S.t.\ \ v(k) - Ta_{\mathrm{x,min}} < v_{\mathrm{x}} < v(k) + Ta_{\mathrm{x,max}}$$

$$-\gamma_{\mathrm{min}} < \gamma < \gamma_{\mathrm{max}}$$

$$\mathcal{G}_{\mathrm{tt,min}} < \mathcal{G}_{\mathrm{a}} < \mathcal{G}_{\mathrm{tt,max}},\ tt = a,\ b$$

$$p_{ij,\mathrm{min}} < p_{ij} < p_{ij,\mathrm{max}}\ \ ij = 1, 2$$

where $\mathcal{G}_{\mathrm{tt,min}}$, $\mathcal{G}_{\mathrm{tt,max}}$, $p_{\mathrm{ij,min}}$ and $p_{\mathrm{ij,max}}$ are the maximum and minimum of the optimized variables. In order to perspicuously manifest the optimization process, the flow is shown in Algorithm 1.

4.2. Tracking-level Controller Design

Denote by $\mathcal{G}$ the output of the LTV system of the vehicle as shown following

$$\mathcal{G}(k) = \begin{bmatrix} 1 & 0 & 0 \\ 0 & 0 & 1 \end{bmatrix} \varsigma(k) \tag{31}$$

Based on the reference states generated by the planning

controller, the cost function at time k in the finite horizon optimal control problem can be expressed as:

$$J_2 : \sum_{i=1}^{H_p} \left\| \vartheta_{k+i,k} - \vartheta^*_{k+i,k} \right\|^2_{\mathcal{P}_2} + \sum_{p=0}^{H_c-1} \left\| \Delta u_{k+p,k} \right\|^2_{\mathcal{Q}_2} \tag{32}$$

where $\mathcal{P}_2$ and $\mathcal{Q}_2$ are definite positive matrices; H_p and H_c are the prediction and control horizons; ϑ^* is the reference states generated by the planning controller. At each time step k, the next finite horizon optimal control problem is solved:

$$\min_{\Delta u_k} J_2 \tag{33}$$

$$S.t.\ \ \varsigma_{k+i,k} = A_k \varsigma_{k,k} + B_k u_{p,k} + d_k$$

$$\vartheta_{rr,k} = \begin{bmatrix} 1 & 0 & 0 \\ 0 & 0 & 1 \end{bmatrix} \varsigma_{rr,k},\ \ rr = k, \ldots,\ k + H_p$$

$$d_k = \bar{f}(T, \bar{\varsigma}_k, \bar{u}_k) - A_k \bar{\varsigma}_k - B_k \bar{u}_k$$

$$\bar{\varsigma}_k = \varsigma_k,\ \ \bar{u}_k = u(k-1)$$

$$u_{pp,k} = u(k-1) + \Delta u_{pp,k},\ \ pp = k, \ldots,\ k + H_c - 1$$

$$\Delta u_{k+p,k} = 0,\ \ p = H_c, \ldots, H_p$$

$$u_{min} \le u_{pp,k} \le u_{max},\ \ \Delta u_{min} \le \Delta u_{pp,k} \le \Delta u_{max}$$

$$\alpha_{j,min} \le \alpha_{j,t,k} \le \alpha_{j,max},\ j = f,\ r$$

where $\Delta u_k \triangleq [\Delta u_{k,k}, \ldots, \Delta u_{k+H_c-1,k}]^T$.

The optimization problem (33) can be modified into a quadratic program (QP) (see Borrelli *et al*. (2005)). Denote by $\Delta u^{\#}_k \triangleq [\Delta u^{\#}_{k,k}, \ldots, \Delta u^{\#}_{k+H_c-1,k}]^T$ the sequence of optimal input deviations computed at time k by solving Equation (33) for the current states $\varsigma(k)$. Then, the first sample $\Delta u^{\#}_k$ is used to compute the optimal control action, and the resulting state feedback control law is

Table 1. Parameters for the experimental vehicles.

Parameter	Value
Vehicle total mass M	1723 kg
Vehicle moment of inertia about the yaw axis I_z	4175 kg.m^2
Distances of the CoG to the front and rear axle l_f and l_r	1.4 m, 1.6 m
Rolling and air resistance coefficient k_r and k_d	0.1, 0.018
Acceleration of gravity g	9.8 m/s^2
Air density ρ	1.206 N.s^2.m^{-4}
Windward area S_d	1.8 m^2
Tire-road adhesion coefficient μ_g	0.8
Tire cornering stiffness C_f and C_r	52700 N/rad, 66900 N/rad
Length of vehicle L_c	2 m

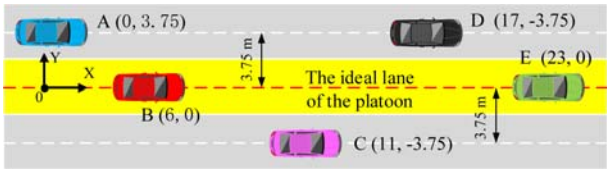

Figure 5. Initial displacements of the vehicles in the homogeneous platoon.

$$u\left(k, \varsigma(k)\right) = u(k-1) + \Delta u^{\#}_{k,k}\left(k, \varsigma(k)\right) \tag{34}$$

At the next time step $k + 1$, the optimization problem (33) is solved over a shifted horizon based on the new measurements of the state $\varsigma(k+1)$ and based on an updated linear model (17) computed by linearizing the nonlinear vehicle model.

Remark 4: Note that, to simplify the subsequent linearization and controller design, we use tire forces as the output of the control system in the control design. The force can be deemed as the required tire force that fulfills a stable vehicle platoon formation. In the actual simulation, the traction/braking torque of wheels are the actual input of the vehicle platform, which can be generated by the tire forces based on the wheel dynamic model.

5. SIMULATION AND RESULTS

To verify the performance of the proposed control system, simulation of five vehicles (named by Vehs. A, B, C, D, and E) is implemented to form the platoon. The ten-DOF four-wheel-independently-drive (4WID) vehicles, by referring to Wang *et al*. (2009), is applied to imitate the real vehicle system in the simulation. The vehicle model consists of three degrees of translational freedom of vehicle body, three degrees of rational freedom, and the rotational motion for each of the four tires. Dugoff's tire model is used to calculate the longitudinal and lateral tire-road friction forces. The main parameters of each vehicle are listed in Table 1.

Initially, the five vehicles occupy different lanes, and the initial positions are described as Figure 5. The velocities of vehicles are set to 18 m/s, 25 m/s, 24 m/s, 22 m/s, and 27 m/s order, and the original yaw angles, yaw rates, lateral velocities, and accelerations are zero. Also, the lane occupied by Vehs. B and E is the preassigned ideal lane of the platoon, the final speed of the platoon is 23 m/s, and the desired inter-vehicle spacing is 10 m. Note that the global coordinate position the ideal lane, where the X-axis points to the direction of the vehicle running along the lane-two and the Y-axis is perpendicular to the X axis pointing to the right.

In addition, to demonstrate the advantage of the proposed control system, another benchmark is also simulated. In the following, *Controller I* refers to the proposed DPFC and *Controller II* refers to the tradition

MOF controller which does not consider the vehicle lateral dynamics. The main parameters in these two controllers are listed:

1) $T = 0.05$ s, $H_p = 4$, $H_c = 2$, $N_t = 4$, $\alpha_{min} = -5$ deg, $\alpha_{max} = 5$ deg;
2) $\mathcal{G}_{a,min} = 0.01$, $\mathcal{G}_{b,min} = 0.01$, $p_{ij,min} = 0.01$, $p_{ij,max} = 2$, $\mathcal{G}_{a,max} = 2$, $\mathcal{G}_{b,max} = 2$.

The simulation results and their performances are shown in Figures 6 ~ 9 and Table 2. Figure 6 is the trajectories of vehicles. The inter-vehicle spacings and longitudinal speeds are shown in Figures 7 and 8. Figure 9 is the dynamic constraints of some vehicles, which need to carry out steering maneuver.

As shown in Figures 6 and 7, Vehs. A, C and D in both controllers complete the lane-changing maneuver at the end of the simulation, and the inter-vehicle spacings converge to 10 m. Note that the spacing of arbitrary contiguous vehicles in two controllers is more significant than L_c (the length of the vehicle) during the platoon formation, which indicates the inter-vehicle collisions do not occur.

It is observed from Figure 8, although the longitudinal speeds of vehicles in two controllers are converging to the 23 m/s at the end, the absolute maximum tracking error of longitudinal speed $|e_{m,v}|$ in *Controller II* is significant. Considering the tracking control levels in the two controllers are identical, large tracking error in *Controller II* may be caused by actuator saturation.

In Figure 9, the yaw rate trajectories of *Controller II* for Vehs. A, C and D are all exceeding the stability boundaries, which indicates the unstable vehicle operation occurs. Also, the trajectories of all vehicles for *Controller I* stay

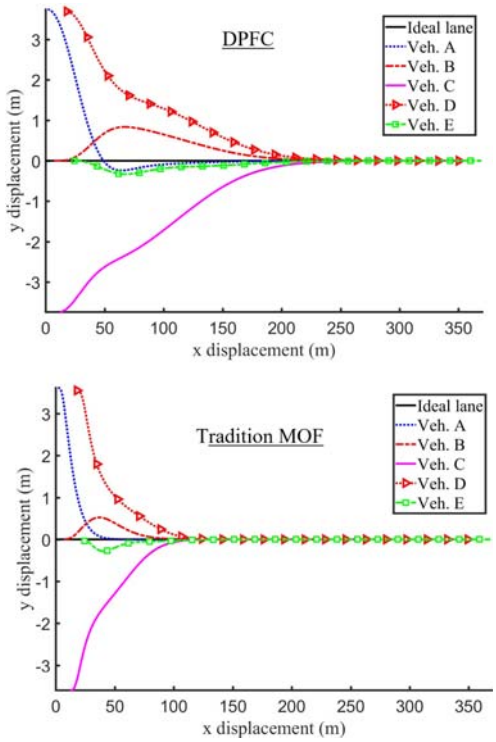

Figure 6. Motion trails of vehicles.

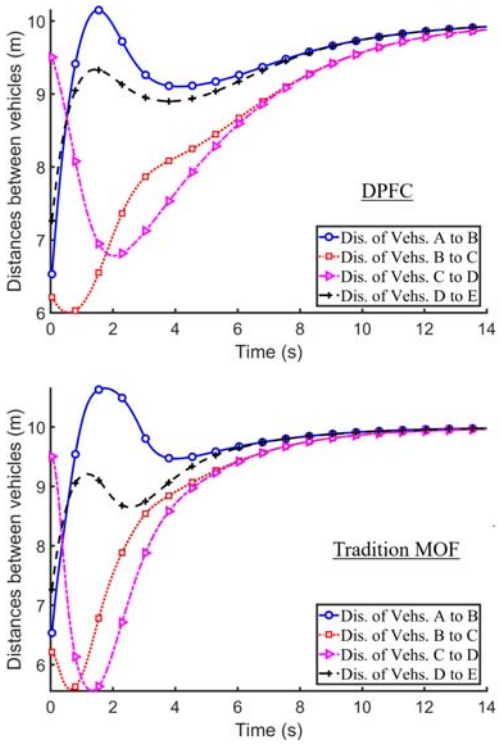

Figure 7. Inter-vehicle spacing.

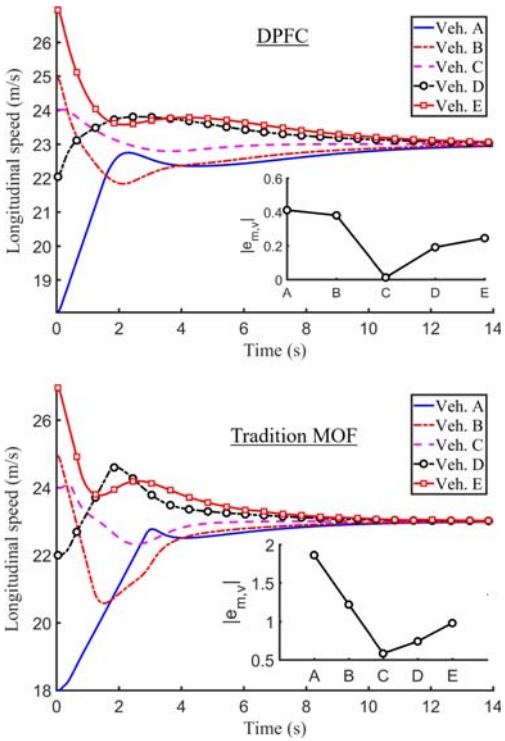

Figure 8. Longitudinal speeds of vehicles.

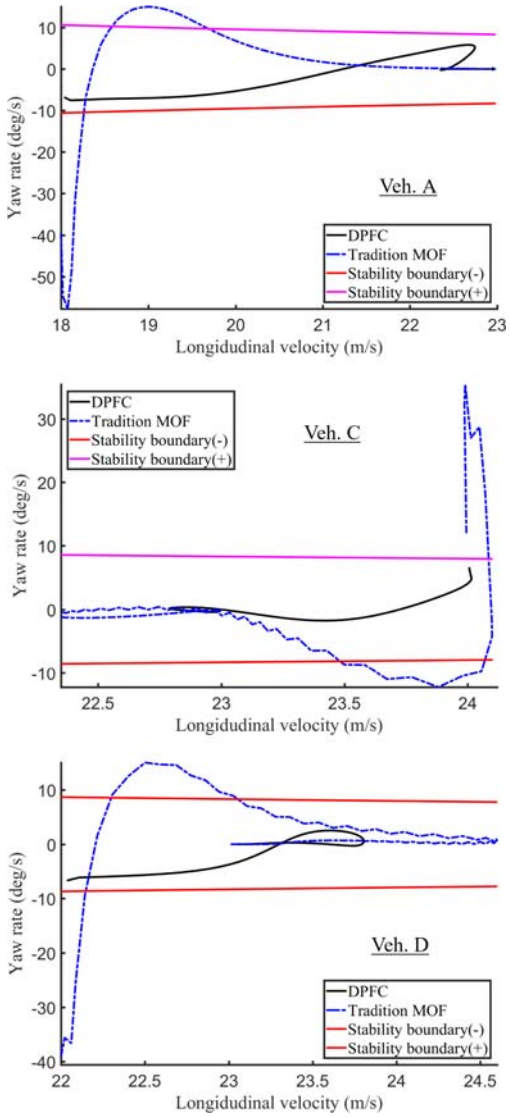

Figure 9. Stability boundary of the vehicle.

within the stable range but may close to the boundaries while the longitudinal speeds are 18 m/s, 24 m/s and 22 m/s. It indicates that the *Controller I* form the vehicle platoon with aggressive strategy but still stable vehicle operations. Thus, vehicle stability and rapidly of platoon formation are guaranteed simultaneously.

Synthesizes the above analysis, we can see from Table 2 that, compared with the traditional controller, although the proposed control algorithm has a slightly longer convergence time in formation, it can achieve accurate speed tracking control and enhance the safety of the vehicle in formation process on the premise of ensuring the stability of the vehicle system.

Table 2. Performances contrast of two controllers.

Controller	CT[1]	AMSTE[2]	MVS[3]	DS[4]
Controller I	14 s	0.4 m	6 m	Stable
Controller II	12 s	2 m	5.5 m	Unstable

[1]Convergence Time. [2]Absolute Maximum Speed Tracking Error. [3]Minimum Vehicle spacing. [4]Vehicle Dynamic Stability

6. CONCLUSION

In this paper, a DPFC framework for HAVs is proposed to achieve stable and efficient platoon formation by combining the MOF and vehicle dynamics. In addition to the vehicle kinematic constraints, vehicle dynamics and actuator saturation are taken into consideration. To ensure the stable vehicle operation, the stability boundaries of each vehicle is calculated and the parameter optimization of MOF is conducted.

The platoon formation with five vehicles is simulated to assess the effectiveness of proposed control systems. The simulation results show that the proposed DPFC can achieve safe platoon formation as well as shorter converge duration compared to the traditional MOF controller.

ACKNOWLEDGEMENT–This work was supported by the National Natural Science Foundation of China under Grants 51575103, U1664258 and 51805081, National Key R&D Program in China under Grants 2016YFB0100906 and 2016YFD0700905, and Scientific Research Foundation of Graduate School of Southeast University under Grant YBJJ1704.

REFERENCES

Antonelli, G. and Chiaverini, S. (2006). Kinematic control of platoons of autonomous vehicles. *IEEE Trans. Robotics* **22**, **6**, 1285–1292.

Al-Jhayyish, A. M. and Schmidt, K. W. (2018). Feedforward strategies for cooperative adaptive cruise control in heterogeneous vehicle strings. *IEEE Trans. Intelligent Transportation Systems* **19**, **1**, 113–122.

Bishop, B. E. (2003). On the use of redundant manipulator techniques for control of platoons of cooperating robotic vehicles. *IEEE Trans. Systems, Man, and Cybernetics - Part A: Systems and Humans* **33**, **5**, 608–615.

Borrelli, F., Falcone, P., Keviczky, T., Asgari, J. and Hrovat, D. (2005). MPC-based approach to active steering for autonomous vehicle systems. *Int. J. Vehicle Autonomous Systems* **3**, **2-4**, 265–291.

Desai, J. P., Ostrowski, J. P. and Kumar, V. (2001). Modeling and control of formations of nonholonomic mobile robots. *IEEE Trans. Robotics and Automation* **17**, **6**, 905–908.

Fax, J. A. and Murray, R. M. (2004). Information flow and cooperative control of vehicle formations. *IEEE Trans. Automatic Control* **49**, **9**, 1465–1476.

Gao, F., Dang, D. F., Huang, S. S. and Li, S. E. (2017). Decoupled robust control of vehicular platoon with identical controller and rigid information flow. *Int. J.*

Automotive Technology **18**, **1**, 157–164.

Iftekhar, L. (2012). *Safety-aware Intelligent Transportation Systems: Cooperative Autonomous Driving for Vehicular Networks*. Ph. D. Dissertation. Dartmouth College. Hanover, New Hampshire, USA.

Jia, Y. (2000). Robust control with decoupling performance for steering and traction of 4WS vehicles under velocity-varying motion. *IEEE Trans. Control Systems Technology* **8**, **3**, 554–569.

Kamal, M. A. S., Imura, J. I., Hayakawa, T., Ohata, A. and Aihara, K. (2014). Smart driving of a vehicle using model predictive control for improving traffic flow. *IEEE Trans. Intelligent Transportation Systems* **15**, **2**, 878–888.

Liu, Y. and Xu, B. (2015). Improved protocols and stability analysis for multivehicle cooperative autonomous systems. *IEEE Trans. Intelligent Transportation Systems* **16**, **5**, 2700–2710.

Naus, G. J., Vugts, R. P., Ploeg, J., van de Molengraft, M. J. and Steinbuch, M. (2010). String-stable CACC design and experimental validation: A frequency-domain approach. *IEEE Trans. Vehicular Technology* **59**, **9**, 4268–4279.

Olfati-Saber, R. (2006). Flocking for multi-agent dynamic systems: Algorithms and theory. *IEEE Trans. Automatic Control* **51**, **3**, 401–420.

Olfati-Saber, R. (2002). Near-identity diffeomorphisms and exponential ε-tracking and ε-stabilization of first-order nonholonomic *SE* (2) vehicles. *Proc. American Control Conf. (ACC)*, Anchorage, Alaska, USA.

Peng, Z., Wen, G., Yang, S. and Rahmani, A. (2016). Distributed consensus-based formation control for nonholonomic wheeled mobile robots using adaptive neural network. *Nonlinear Dynamics* **86**, **1**, 605–622.

Ploeg, J., Shukla, D. P., van de Wouw, N. and Nijmeijer, H. (2014). Controller synthesis for string stability of vehicle platoons. *IEEE Trans. Intelligent Transportation Systems* **15**, **2**, 854–865.

Rajamani, R. (2012). *Vehicle Dynamics and Control*. 2nd edn. Springer. Boston, Massachusetts, USA.

Swaroop, D. V. A. H. G., Hedrick, J. K., Chien, C. C. and Ioannou, P. (1994). A comparision of spacing and headway control laws for automatically controlled vehicles. *Vehicle System Dynamics: Int. J. Vehicle Mechanics and Mobility* **23**, **1**, 597–625.

Wang, C. and Nijmeijer, H. (2015). String stable heterogeneous vehicle platoon using cooperative adaptive cruise control. *Proc. IEEE 18th Int. Conf. Intelligent Transportation Systems*, Las Palmas, Spain.

Wang, J. X., Chen, N., Pi, D. W. and Yin, G. D. (2009). Agent-based coordination framework for integrated vehicle chassis control. *Proc. Institution of Mechanical Engineers, Part D: J. Automobile Engineering* **223**, **5**, 601–621.

World Health Organization (2015). Global Status Report on Road Safety 2015.

Xu, L., Zhuang, W., Yin, G. and Bian, C. (2018). Stable longitudinal control of heterogeneous vehicular platoon with disturbances and information delays. *IEEE Access*, **6**, 69794–69806.

Xu, L., Zhuang, W., Yin, G., Li, G. and Bian, C. (2019). Simultaneous longitudinal and lateral control of vehicle platoon subject to stochastic communication delays. *J. Dynamic Systems, Measurement, and Control* **141**, **4**, 044503-1–044503-13.

Yang, S., Cao, Y., Peng, Z., Wen, G. and Guo, K. (2017). Distributed formation control of nonholonomic autonomous vehicle via RBF neural network. *Mechanical Systems and Signal Processing* **87**, **Part B**, 81–95.

Yu, X. and Liu, L. (2016). Distributed formation control of nonholonomic vehicles subject to velocity constraints. *IEEE Trans. Industrial Electronics* **63**, **2**, 1289–1298.

Zhang, J., Wang, F. Y., Wang, K., Lin, W. H., Xu, X. and Chen, C. (2011). Data-driven intelligent transportation systems: A survey. *IEEE Trans. Intelligent Transportation Systems* **12**, **4**, 1624–1639.

Zhang, Q., Lapierre, L. and Xiang, X. (2013). Distributed control of coordinated path tracking for networked nonholonomic mobile vehicles. *IEEE Trans. Industrial Informatics* **9**, **1**, 472–484.

Zheng, Y., Li, S. E., Li, K. and Wang, L. Y. (2016). Stability margin improvement of vehicular platoon considering undirected topology and asymmetric control. *IEEE Trans. Control Systems Technology* **24**, **4**, 1253–1265.

Zhou, J. and Peng, H. (2005). Range policy of adaptive cruise control vehicles for improved flow stability and string stability. *IEEE Trans. Intelligent Transportation Systems* **6**, **2**, 229–237.